PAPER

Check for updates

Rhodamine 6G hydrazone with coumarin unit: a novel single-molecule multianalyte (Cu^{2+} and Hg^{2+}) sensor at different pH value†

Zhou-Qing Xu, Xian-Jie Mao, Yuan Wang,* Wei-Na Wu,* Pan-Dong Mao, Xiao-Lei Zhao, Yun-Chang Fan and Hui-Jun Li*

A rhodamine derivative was synthesised *via* the hydrazone formation of rhodamine 6G hydrazide with 7-diethylamino-3-(1-hydroxy-3-oxobut-1-enyl)-2*H*-chromen-2-one. As a colourimetric and ratiometric fluorescent probe, the derivative exhibited high selectivity towards Cu^{2+} in neutral aqueous media. Moreover, the probe sensed Hg^{2+} with fluorescence enhancement at pH 10. The binding process was confirmed *via* UV-vis absorption, fluorescence measurements, ^{1}H NMR, mass spectroscopy and density functional theory calculation. To validate the applicability of the probe, the probe was used to detect Cu^{2+} and Hg^{2+} ions in actual water samples. The application of the fluorescent sensor in monitoring intracellular Cu^{2+} in Hela cells has also been demonstrated.

Introduction

Cu^{2+} has an important role in the biological systems of plants, living cells and humans. High Cu^{2+} concentrations, however, cause oxidative stress and disorders that are associated with neurodegenerative diseases, such as Alzheimer's, Wilson's and Menke's diseases.[1-3] Given the significant physiological relevance and associated biomedical implications of Cu^{2+}, methods for the highly selective and sensitive detection of Cu^{2+} ions are crucial.[4-6] Cu^{2+} ions have been detected using several analytical techniques, including atomic absorption spectrometry,[7] inductively coupled plasma atomic emission spectrometry,[8] voltammetry and electrochemical methods.[9,10] Nonetheless, these methods are complex, time consuming and/or need special equipment. In addition, they require complicated sample preparation and Cu^{2+} extraction *via* tissue or cell destruction; therefore, these methods are unsuitable for living biosystems.[11] Due to their high selectivity and sensitivity, fluorescent probes have been widely applied in recent years for the detection of anions, cations and biological molecules and for real-time imaging.[11-14]

The rhodamine framework is extensively used as a chemosensor due to its excellent photophysical properties, such as long absorption and emission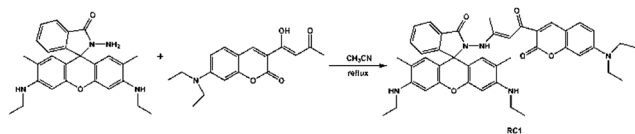 wavelengths, high fluorescence quantum yield, high extinction coefficient and high photostability.[15] Selective chemiluminescence, colorimetric and fluorescence turn-on rhodamine-based sensors, especially rhodamine hydrazones for Cu^{2+} have been successfully developed.[15-30] Nevertheless, various factors, such as instrumental efficiency, environmental condition and probe concentration, interfere with the performance of turn-on probes.[31,32] Accordingly, some ratiometric fluorescent probes for Cu^{2+} containing rhodamine and coumarin,[33,34] indole,[35,36] cyanine,[37] pyrene[38] or naphthalimide[32] groups have been reported to alleviate this problem through guest-induced fluorescence resonance energy transfer (FRET) or bond energy transfer (BET) mechanism. Some of these probes, however, require complicated synthesis procedures that involve harsh reaction conditions and expensive chemicals.[32]

A novel design concept of a single chemosensor for multiple analytes has recently emerged.[18] The detection methods for numerous metal ions with differential responses are more efficient and less expensive than one-to-one analytical methods.[38-41] Hg^{2+} is one of the most toxic metal ions. When present in soil or effluent water, Hg^{2+} is assimilated and converted by lower-order aquatic organisms into methylmercury, which is one of the most potent neurotoxins to humans.[42-46] Therefore, the development of a new fluorescent probe for the simultaneous detection of Cu^{2+} and Hg^{2+} is highly desirable.

Although many rhodamine-based dual-function fluorescent chemosensors for Cu^{2+} and Hg^{2+} are available,[18,34,39,47,48] the selective detection of Cu^{2+} and Hg^{2+} at different pH conditions is rarely reported.[48] Coumarin dye exhibits excellent photochemical and photophysical properties, and has a low toxicity to the environment and the human body. Several coumarin-based chemosensors exhibit effective fluorescence enhancement for

College of Chemistry and Chemical Engineering, Henan Polytechnic University, Jiaozuo 454000, P. R. China. E-mail: wangyuan08@hpu.edu.cn; wuwn08@hpu.edu.cn; lihuijunxgy@hpu.edu.cn

† Electronic supplementary information (ESI) available: ^{1}H NMR ESI-MS spectrum and other additional figures for the probe. CCDC 1509525. For ESI and crystallographic data in CIF or other electronic format see DOI: 10.1039/c7ra05424f

Paper

Scheme 1 Synthesis route of the sensor **RC1**.

Fig. 1 The crystal structure of **RC1**·1.5CH$_3$CN, symmetry code: (i) 3 − x, 2 − y, −z.

the recognition of Hg^{2+}.[49,50] Meanwhile, some coumarin β-diketones have been used as on–off fluorescent chemosensors to selectively detect Cu^{2+}.[51,52] Thus, in this paper, we report **RC1** (Scheme 1). Under neutral conditions, **RC1** acts as a ratiometric fluorescent probe for Cu^{2+} *via* hydrolysis. In a basic environment (pH 10), **RC1** acts as a fluorescence-enhanced probe towards Hg^{2+} *via* the coordination mechanism. **RC1** is easily prepared *via* a simple Schiff base condensation reaction. The application of the fluorescent sensor was further used for detecting Cu^{2+} and Hg^{2+} ions in actual water samples, and for imaging of Cu^{2+} in living cells.
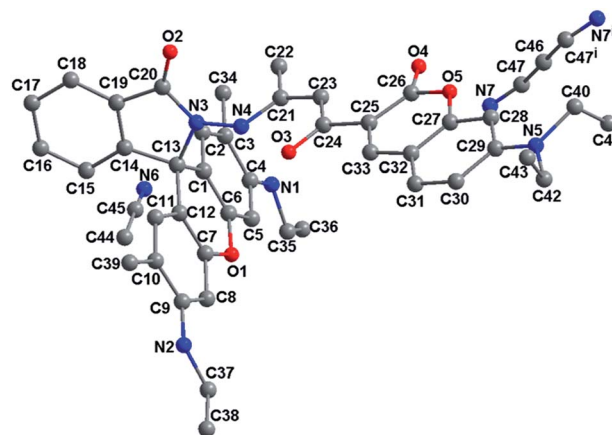
Experimental section

Materials and instrumentation

Solvents and starting materials for synthesis were purchased commercially and used as received. Rhodamine 6G hydrazide and 7-diethylamino-3-(1-hydroxy-3-oxobut-1-enyl)-2H-chromen-2-one were synthesized according to the literature methods.[27,51] The melting point of the probe is determined on an XT4-100X microscopic melting point apparatus (made in Beijing, China). Elemental analyses were carried out on an Elemental Vario EL analyzer. ^{1}H NMR and ^{13}C NMR spectra are recorded on a Bruker AV400 NMR spectrometer in DMSO-d_6 solution. The UV spectra were recorded on a Purkinje General TU-1800 spectrophotometer. Fluorescence spectra were determined on a Varian CARY Eclipse spectrophotometer, in the measurements of emission and excitation spectra the pass width is 5 nm. ESI-MS spectra were obtained on a Bruker Daltonics Esquire 6000 mass spectrometer. The X-ray diffraction measurement for **RC1**·1.5CH$_3$CN was performed on a Bruker SMART APEX II CCD diffractometer equipped with a graphite monochromatized MoKα radiation (λ = 0.71073 Å) by using φ–ω scan mode. Semi-empirical absorption correction was applied to the intensity data using the SADABS program.[53] The structure was solved by direct method and refined by full matrix least-square on F^2 using the SHELXTL-97 program.[54] All non-hydrogen atoms were refined anisotropically. Except for one half of crystal CH$_3$CN, all the other H atoms were positioned geometrically and refined using a riding model.

Synthesis of RC1

A quantity of rhodamine 6G hydrazide (428 mg, 1 mmol) was added to a CH$_3$CN solution (20 mL) containing 7-diethylamino-3-(1-hydroxy-3-oxobut-1-enyl)-2H-chromen-2-one (301 mg, 1 mmol). The mixture was refluxed for 12 h with three drops of acetic acid. The separated solid was filtered, washed with CH$_3$CN, and then recrystallized in CH$_3$CN solution. Yield 45%.

Mp 212–216 °C. Anal. calc. for C$_{43}$H$_{45}$N$_5$O$_5$: C, 72.55; H, 6.37; N, 9.84. Found: C, 72.66; H, 6.22; N, 10.02%. ^{1}H NMR (400 MHz, DMSO-d_6), δ (ppm): 11.75 (s, 1H, NH), 8.42 (s, 1H, aryl-H), 7.98–8.00 (d, 1H, aryl-H, J = 7.2 Hz), 7.64–7.74 (m, 3H, aryl-H), 7.19–7.21 (d, 1H, aryl-H, J = 2.0 Hz), 6.79–6.81 (dd, 1H, aryl-H, J = 7.2, 2.0 Hz), 6.58–6.59 (d, 1H, aryl-H, J = 7.2 Hz), 6.32 (s, 2H, aryl-H), 6.27–6.28 (d, 3H, 2aryl-H & CH), 5.23–5.26 (t, 2H, 2NH–CH$_2$, J = 5.2 Hz), 3.50–3.55 (q, 4H, 2CH$_2$, J = 7.2 Hz), 3.17–3.23 (m, 4H, 2CH$_2$), 1.98 (s, 6H, 2CH$_3$), 1.26–1.30 (t, 6H, 2CH$_3$, J = 7.2 Hz), 1.17–1.20 (t, 6H, 2CH$_3$, J = 6.8 Hz). ESI-MS: m/z = 712.3800 for [M + H]$^+$, 356.6962 for [M + 2H]$^{2+}$. Crystal data for **RC1**·1.5CH$_3$CN (C$_{46}$H$_{49.5}$N$_{6.5}$O$_5$, Fig. 1): crystal size: 0.10 × 0.10 × 0.04 mm, triclinic, space group P$\bar{1}$. a = 10.543(8) Å, b = 11.218(9) Å, c = 19.322(16) Å, α = 85.354(17)°, β = 74.292(15)°, γ = 78.481(16)°, V = 2155(3) Å^3, Z = 2, T = 296(2) K, θ = 1.85–25.00°, 10 993 reflections measured, 7551 unique (R_{int} = 0.0892). Final residual for 530 parameters and 7551 reflections with $I > 2\sigma(I)$: R_1 = 0.0731, wR_2 = 0.1166 and GOF = 1.028.

General UV-vis and fluorescence spectra measurements

The spectral analyses were accomplished at room temperature in CH$_3$CN/H$_2$O (9/1, v/v, pH = 7.4) solution for Cu^{2+} detection, while in CH$_3$CN/H$_2$O (9/1, v/v, pH = 10.0) solution in the case of Hg^{2+}. The concentration of the probe **RC1** for UV-vis and fluorescence measurement was 5 μM. Solutions of metal ions were prepared with nitrate or chloride salts in CH$_3$CN. UV-vis and fluorescence spectrophotometric titration were conducted directly in 2 mL cuvette by successive addition of corresponding chemical reagent using a microliter syringe. Upon addition of every aliquot, the solution was well mixed then the spectrum was measured.

Results and discussions

Detection of Cu^{2+} in CH$_3$CN/H$_2$O (9/1, v/v, pH = 7.4) solution using RC1

The selectivity of the **RC1** probe for various metal cations was investigated. As shown in Fig. 2, the free **RC1** sensor (5 μM) in CH$_3$CN/H$_2$O (9/1, v/v, pH = 7.4) solution features two

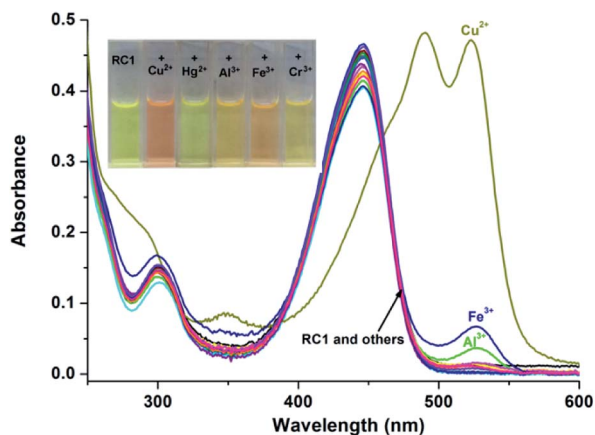**Fig. 2** UV-vis spectra of 5 μM probe **RC1** in CH$_3$CN/H$_2$O (9/1, v/v, pH = 7.4) solution with 5 equiv. of metal ions: Ag$^+$, Al^{3+}, Ca^{2+}, Cd^{2+}, Co^{2+}, Cr^{3+}, Cu^{2+}, Fe^{3+}, Hg^{2+}, K$^+$, Mg^{2+}, Mn^{2+}, Na$^+$, Ni^{2+}, Pb^{2+} and Zn^{2+} ions and blank. The inset shows the change of the color with the addition of Cu^{2+} to **RC1** solution.

absorption bands at 300 and 445 nm, which could be assigned to the π–π* transition of rhodamine in a spirocycle-closed form and to the coumarin moiety,[27,51] respectively. Upon the addition of 5 equiv. Cu^{2+} to the **RC1** solution, the mixture exhibited a significant absorbance at 520 nm corresponding to the orange colour. However, in the case of other metal cations, only trivalent metal ions (Al^{3+}, Cr^{3+} and Fe^{3+}) induced a slight absorbance enhancement at 520 nm (approximately 14% of Cu^{2+} in the case of Fe^{3+}). Other cations, such as Ag$^+$, Ca^{2+}, Cd^{2+}, Co^{2+}, Hg^{2+}, K$^+$, Mg^{2+}, Mn^{2+}, Na$^+$, Ni^{2+}, Pb^{2+} and Zn^{2+} ions, exerted almost no influence on the absorption of **RC1**. This result indicated that under neutral conditions, **RC1** is a visible colourimetric probe that is selective for Cu^{2+}.

Under excitation at 445 nm, the free **RC1** probe displayed one fluorescence emission band at 498 nm (Fig. 3) because of
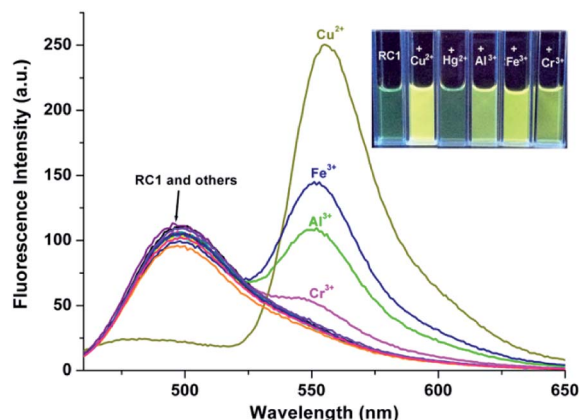
the coumarin fluorophore.[31,51] Upon the addition of 5 equiv. Cu^{2+}, the emission band at 498 nm drastically decreased. By contrast, the other metal ions exerted no influence on the same emission band. In addition, Cu^{2+} caused a clear fluorescence enhancement of **RC1** at 550 nm, corresponding to the yellow colour under a 365 nm UV lamp. The strong Lewis acidity of Al^{3+}, Cr^{3+} and Fe^{3+} likely induced the hydrolytic cleavage of the imine bond, thus triggering the fluorescence emission of **RC1** at 550 nm.[55] The variety of fluorescence intensity ratio F_{550}/F_{498}, however, is highly selectively for Cu^{2+} (Fig. S1, ESI†). Therefore, **RC1** is also a ratiometric fluorescent probe towards Cu^{2+}.

To obtain further information on the binding form of the **RC1** sensor with Cu^{2+}, absorption and fluorescence spectrum titrations were performed. As shown in Fig. 4, the absorbance peak at 520 nm was significantly enhanced upon the gradual addition of up to 8 equiv. Cu^{2+} to 5 μM **RC1** sensor in CH$_3$CN/H$_2$O (9/1, v/v, pH = 7.4) solution; this result indicated that the spirolactam ring opened due to Cu^{2+} addition.[28] Moreover, upon the addition of Cu^{2+}, the absorbance at 350 and 294 nm gradually increased, whereas that at 445 nm decreased. The three isosbestic points at 461, 385 and 335 nm suggested that **RC1** may decompose into several components that exist in equilibrium.[55] Furthermore, the absorbance at 520 nm (Fig. 4, inset) increased linearly over the Cu^{2+} concentration range of 0–30 μM.

The FRET pathway was completely suppressed in the free probe **RC1** probe, and only an emission maximum near 498 nm was observed when the probe was excited at 445 nm. The emission at 498 nm decreased upon the addition of <1 equiv. Cu^{2+}. However, upon the addition of >1 equiv. Cu^{2+}, the emission band with a λ_{max} near 498 nm decreased and was accompanied by the generation of a new fluorescence band at 550 nm (Fig. 5). The linear response range of the fluorescence intensity ratios (F_{550}/F_{498}) covered a Cu^{2+} concentration range of 8–15 μM (Fig. 5, inset). Evidently, the binding of the receptor to Cu^{2+} induced the FRET process, which produced an intense rhodamine-based yellow emission, *i.e.*, energy transfer from coumarin to xanthene resulted
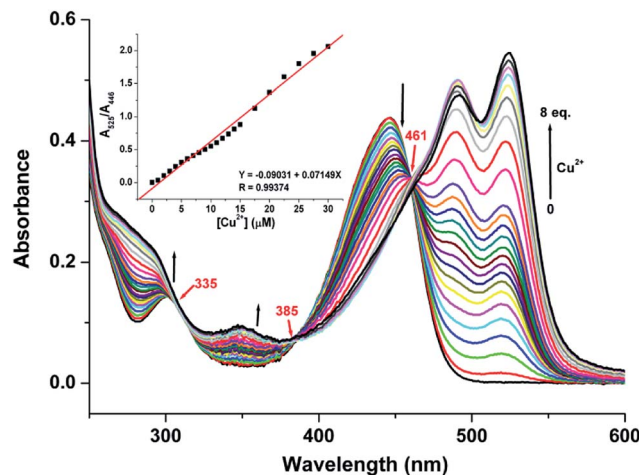

Fig. 3 Fluorescence emission spectra of 5 μM probe **RC1** in CH$_3$CN/H$_2$O (9/1, v/v, pH = 7.4) solution with 5 equiv. of metal ions: Ag$^+$, Al^{3+}, Ca^{2+}, Cd^{2+}, Co^{2+}, Cr^{3+}, Cu^{2+}, Fe^{3+}, Hg^{2+}, K$^+$, Mg^{2+}, Mn^{2+}, Na$^+$, Ni^{2+}, Pb^{2+} and Zn^{2+} ions and blank, excitation wavelength was 445 nm. The inset shows the change of the color with the addition of Cu^{2+} to **RC1** under 365 nm UV lamp.

Fig. 4 Absorption spectra of 5 μM probe **RC1** upon the addition of Cu^{2+} (0–8 equiv.) in CH$_3$CN/H$_2$O (9/1, v/v, pH = 7.4) solution. The inset shows the linear response range of the absorbance at 520 nm as a function of Cu^{2+} concentration (0–30 μM).
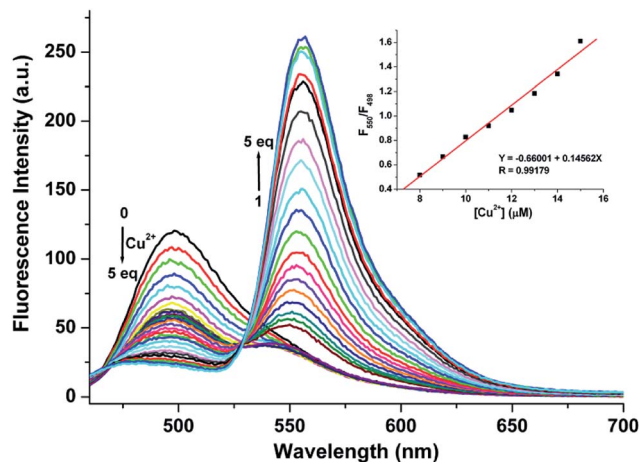
Fig. 5 Fluorescence emission spectra of 5 μM probe **RC1** upon the addition of Cu^{2+} (0–5 equiv.) in CH_3CN/H_2O (9/1, v/v, pH = 7.4) solution. The inset shows the linear response range of the fluorescence intensity ratio at 550 and 498 nm (F_{550}/F_{498}) as a function of Cu^{2+} concentration (8–15 μM). Excitation wavelength was 445 nm.

Fig. 6 Fluorescence emission spectra of 5 μM probe **RC1** in CH_3CN/H_2O (9/1, v/v, pH = 10.0) solution with 5 equiv. of metal ions: Ag^+, Al^{3+}, Ca^{2+}, Cd^{2+}, Co^{2+}, Cr^{3+}, Cu^{2+}, Fe^{3+}, Hg^{2+}, K^+, Mg^{2+}, Mn^{2+}, Na^+, Ni^{2+}, Pb^{2+} and Zn^{2+} ions and blank, excitation wavelength was 445 nm. The inset shows the change of the color with the addition of Hg^{2+} to **RC1** under 365 nm UV lamp.

from ringopening, thus increasing the overlap integral between the coumarin and xanthene moieties (Fig. S2, ESI†).

Results of the titration experiment revealed that the fluorescence calibration values were normalised between the minimum and the maximum intensities. A linear regression curve was then fitted to the normalised data, and the point at which the regression curve crossed the ordinate axis was considered as the detection limit.[24] Results showed that the detection limit of **RC1** for Cu^{2+} is 6.88 μM (Fig. S3, ESI†), which is considerably lower than the standard value for Cu^{2+} (20 μM) in drinking water recommended by the U.S. EPA.[47] This result indicated that the **RC1** sensor has potential applications as a Cu^{2+} detector in live cell or water samples.

Detection of Hg^{2+} in CH_3CN/H_2O (9/1, v/v, pH = 10.0) solution using RC1

Highly selective probes for Hg^{2+}, which exhibit positive responses instead of fluorescent quenching upon analyte binding, are preferred to promote sensitivity.[34] In CH_3CN/H_2O (9/1, v/v, pH = 10.0) solution, **RC1** displayed high selectivity towards Hg^{2+} due to emission enhancement. The other tested ions exhibited no significant fluorescence changes (Fig. 6). Upon the addition of approximately 17 equiv. Hg^{2+} to 5 μM **RC1**·CH_3CN/H_2O (9/1, v/v, pH = 10.0) solution, the emission band centered at 498 nm (with an excitation wavelength at 445 nm) developed and slightly blue shifted to 490 nm (Fig. 7). Fluorescence intensity increased linearly in the Hg^{2+} concentration range of 0–20 μM (Fig. 7, inset) and the detection limit of **RC1** for Hg^{2+} was 2.96 μM (Fig. S4, ESI†). Moreover, Job's plot experiment, which was evaluated from the absorption spectra, suggested that the binding of **RC1** to Hg^{2+} is of 1 : 1 stoichiometry. The emission intensity was at its peak when the molecular fraction of Hg^{2+} was close to 0.5 (Fig. S5, ESI†). Fitting data to the Benesi–Hildebrand expression showed that the
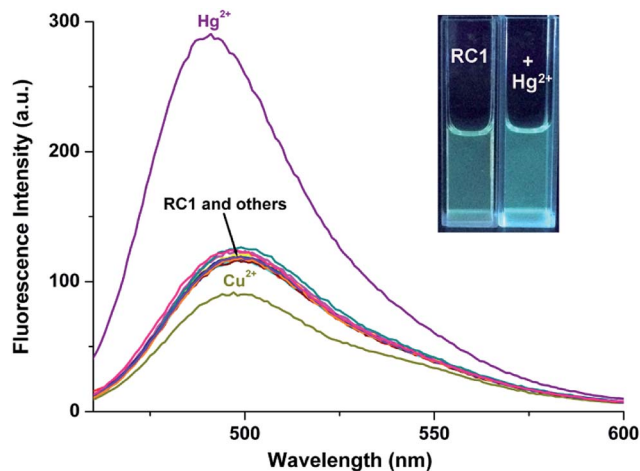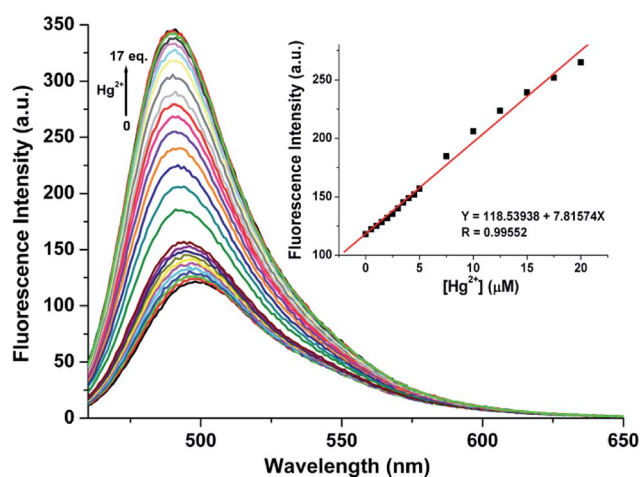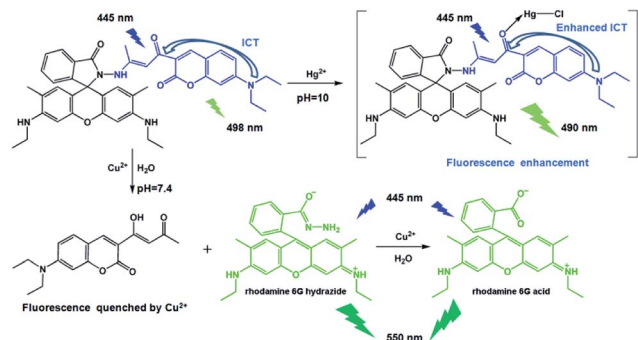

Fig. 7 Fluorescence emission spectra of 5 μM probe **RC1** upon the addition of Hg^{2+} (0–17 equiv.) in CH_3CN/H_2O (9/1, v/v, pH = 10.0) solution. The inset shows the linear response range of the fluorescence intensity at 498 nm as a function of Hg^{2+} concentration (0–20 μM). Excitation wavelength was 445 nm.

binding constant of **RC1** with Hg^{2+} was 3.34×10^4 M^{-1} with a good linear relationship ($R = 0.99768$, Fig. S6 and ESI†).

Reaction mechanism of RC1 with Cu^{2+} and Hg^{2+}

To explore the reaction mechanism of **RC1** with Cu^{2+} or Hg^{2+}, ESI-MS analysis (Fig. S7 and S8, ESI†) was performed. Results showed that upon the addition of Cu^{2+} to an acetonitrile solution of **RC1**, peaks were observed at m/z 429.2259 and 415.2105, which were assigned to rhodamine 6G hydrazide and rhodamine 6G acid, respectively. This result indicated that Cu^{2+} facilitates the hydrolysis of **RC1**, which results in the colour change and visible fluorescence emission at 550 nm (Scheme 2).

Scheme 2 The proposed reaction mechanism of **RC1** with Cu^{2+} and Hg^{2+}.

The hydrolysis mechanism has been demonstrated by Czarnik et al.[2] The fluorescence emission of the coumarin moiety at 498 nm was quenched by excess Cu^{2+} ions but negligibly changed in the presence of Al^{3+}, Cr^{3+} and Fe^{3+}, although these three ions could also catalyse the **RC1** hydrolysis. This result is in agreement with that in literature.[51,52] However, the peaks of Hg^{2+} at m/z 948.2655 were attributed to the $[\text{RC1} + \text{Hg} + \text{Cl}]^+$ complex. The differences in the ^{1}H NMR spectra of **RC1** and **RC1** + Hg^{2+} are also depicted in Fig. S9, ESI.† Upon the addition of Hg^{2+}, the proton peaks at 8.423, 6.583–6.590 and 6.785–6.814 ppm, which are attributable to the coumarin moieties in **RC1**, shifted to the high field, whereas the peak at 6.320 ppm that belongs to rhodamine shifted to low field. Therefore, **RC1** could chelate Hg^{2+} through the O atom of coumarin 3-acyl group, thereby forming a 1 : 1 complex (Scheme 2). In addition, the slight shifts showed that the Hg–O coordination bond is relatively weak. It should be noted that there exists strong intramolecular N–H···O hydrogen bond between the N atom of rhodamine hydrazone and O atom of 3-carbonyl of coumarin (N···O distance being 2.627(5) Å), which will restrict the coordination of Hg^{2+} ions under neutral condition. On the contrary, according to the literature, the carbonyl of rhodamine hydrazone of **RC1** is prefer to participate the coordination with Cu^{2+} ions,[58] thus leading to the hydrolysis process.

To understand the configuration of **RC1** and the $[\text{RC1} + \text{Hg} + \text{Cl}]^+$ complex, we performed density functional theory (DFT) calculations.[56] As shown in Fig. 8, the structure of **RC1** clearly exhibits the distinct spirolactam ring formation of the rhodamine moiety with only coumarin fluorescence emission. In the $[\text{RC1} + \text{Hg} + \text{Cl}]^+$ structure, Hg^{2+} coordinated with the O atom of the coumarin 3-acyl group and one chloride anion, and the Hg–O and Hg–Cl bond lengths were 2.169 and 2.386 Å, respectively. The coordination of the acyl O atom in the 3-position increased its electron withdrawing effect; consequently, the fluorescence intensity of coumarin (accompanied by a slight blue shift) considerably increased through the enhanced ICT process.[50] The spatial distributions and orbital energies of the HOMO and LUMO of **RC1** and the $[\text{RC1} + \text{Hg} + \text{Cl}]^+$ complex were also generated (Fig. 8). The HOMO and LUMO of the **RC1**–Hg^{2+} complex were more stable than those of **RC1**. HOMO and LUMO were both centered on the coumarin moiety in **RC1**. In the case of the **RC1**–Hg^{2+} complex, HOMO localised on half of the
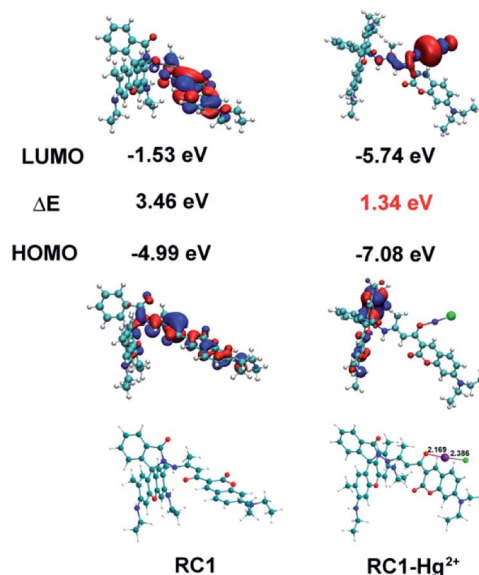

Fig. 8 Optimized structures and HOMO/LUMO of **RC1** and **RC1**–Hg^{2+} complex by DFT calculation.

xanthene backbone. By contrast, the π electrons in the LUMO of the **RC1**–Hg^{2+} complex were located around the Hg^{2+} centre. The calculated energy gap between the HOMO and LUMO of the **RC1**–Hg^{2+} complex was 1.34 eV, which is significantly lower than that of **RC1** (3.46 eV). This result revealed that the binding of Hg^{2+} to the probe stabilizes the system.

Effect of environmental factors and kinetic assay

The pH value is the primary factor that affects the response of the rhodamine-based chemosensor.[28] The spectrum response of **RC1** (5 μM) with or without Cu^{2+}/Hg^{2+} (5 equiv. of each) in CH_3CN/H_2O (9/1, v/v) solutions with different pH values was evaluated at room temperature. Results showed that **RC1** detected Cu^{2+} and Hg^{2+} ions under relatively acidic (pH 4.0–7.6, Fig. S10, ESI†) and basic (pH 10.0–11.0, Fig. S11, ESI†) conditions, respectively. The interference of the coexistent metal cations was also studied. Results showed that except for Al^{3+}, Cr^{3+} and Fe^{3+}, the coexistent metal cations, including Ag^+, Ca^{2+}, Cd^{2+}, Co^{2+}, Hg^{2+}, K^+, Mg^{2+}, Mn^{2+}, Na^+, Ni^{2+}, Pb^{2+} and Zn^{2+} ions, hardly affected the detection of Cu^{2+} (Fig. S12, ESI†). By contrast, the coexistent metal cations exerted no influences on Hg^{2+} detection (Fig. S13, ESI†).

The chemosensor property of short response time is as important as high sensitivity and selectivity.[37] To monitor the target metal ions in real time, the time courses of response to fluorescence changes in **RC1** (5 μM) with 5 equiv. of Cu^{2+} or Hg^{2+} were investigated. As shown in Fig. S14 in ESI,† the fluorescence ratio (F_{550}/F_{498}) immediately increased in Cu^{2+} and stabilised within 1 min, which is a significantly shorter analysis time for Cu^{2+} detection than with the rhodamine B hydroxylamide probe (response time, 2 h).[29] By contrast, the fluorescence intensity of **RC1** + Hg^{2+} stabilised after 2 min (Fig. S15 and

ESI†), which indicated faster detection than with the glyoxylic acid rhodamine B hydrazone probe (response time, 1 h).[57]

Reversibility is an important aspect in the wide application of a chemical sensor for Cu^{2+} or Hg^{2+} detection in specific environments. Thus, we carried out reversibility experiments. As shown in Fig. S16 and ESI,† EDTA chelation with Cu^{2+} recovered coumarin fluorescence but did not influence the rhodamine emission of RC1 + Cu^{2+} at 550 nm. This result provided further evidence for the hydrolysis process of RC1 with Cu^{2+}. By contrast, when 5 equiv. Na_2EDTA was added to 5 μM RC1 probe in CH_3CN/H_2O (9/1, v/v, pH = 10.0) solution with 5 equiv. Hg^{2+}, the fluorescence of the system was quenched. The consecutive additions of Hg^{2+} and Na_2EDTA revealed that this on/off cycle could be repeated (Fig. S17 and ESI†). This observation confirmed that the Hg^{2+} and Na_2EDTA recognition processes are reversible and supported the coordination reaction of RC1 with Hg^{2+}.

Fluorescence imaging of intercellular Cu^{2+}

The ability of the fluorescence chemosensor RC1 to detect Cu^{2+} in Hela cells was examined. The cells were supplemented with RC1 (10 μM) in Dulbecco's modified Eagle's medium (DMEM) supplemented with 10% fetal bovine serum for 0.5 h at 37 °C, leading to intense fluorescence in the blue channel (Fig. 9a) and weak fluorescence in the green channel (Fig. 9b). However, treatment of Cu^{2+} (20 μM) with RC1-loaded cells elicited a partial fluorescence decrease in the blue channel (Fig. 9e) and strong fluorescence in the green channel (Fig. 9f). The results suggest that sensor RC1 can be used to image intracellular Cu^{2+} in living cells.

Practical applications

To verify the practical applicability of the sensors, the standard addition method was utilized to detect Cu^{2+} or Hg^{2+} in distilled water (Kangshifu brand drinking water obtained from the local supermarket) and natural water (obtained from XinYue Lake of

Table 1 Determination of Cu^{2+} and Hg^{2+} concentrations in real water samples ($n = 3$)

Analyte	Sample	Spiked (μM)	Found[a] (μM)	Recovery (%)
Cu^{2+}	Distilled water	0	0	—
		10	9.68 ± 0.15	96.8
		15	14.44 ± 0.08	94.1
	Drinking water[b]	0	0	—
		10	9.52 ± 0.15	95.2
		15	14.39 ± 0.12	95.9
	Natural water[c]	0	0	—
		10	9.48 ± 0.35	94.8
		15	13.98 ± 0.17	93.2
Hg^{2+}	Distilled water	0	0	—
		5	4.86 ± 0.04	97.2
		10	9.88 ± 0.06	98.8
	Drinking water	0	0	—
		5	4.77 ± 0.05	95.4
		10	9.66 ± 0.08	96.6
	Natural water	0	0	—
		5	4.58 ± 0.06	91.6
		10	9.52 ± 0.05	95.2

[a] Average value of three determinations. [b] Kangshifu Drinking water (obtained from the local supermarket): $[K^+]$ = 25.64–700 μM; $[Mg^{2+}]$ = 4.17–203.12 μM; $[Cl^-]$ = 281.69–769 μM; $[SO_4{}^{2-}]$ = 4.17–71 μM. [c] Obtained from XinYue Lake of Henan Polytechnic University.

Henan Polytechnic University).[33] Briefly, 0.2 mL Cu^{2+}- or Hg^{2+}-spiked water sample was mixed with 1.8 mL CH_3CN. The pH value was adjusted to 7.4 and 10.0 for the detection of Cu^{2+} and Hg^{2+}, respectively. Subsequently, 10 μL of 1 mM probe-CH_3CN solution was added, and the fluorescence spectra were recorded. Cu^{2+} and Hg^{2+} concentrations were calculated using the equation shown in Fig. 4 (inset) and 6 (inset), respectively. The obtained recovery was 91.4–98.8%, which indicated the appreciable practicality of the presented sensor (Table 1).

Conclusion

We developed an effective fluorescent ratiometric probe for Cu^{2+}-containing rhodamine and coumarin dyes under neutral condition. The probe could sense Hg^{2+} with fluorescence enhancement at high pH value. Furthermore, the detection of Cu^{2+} and Hg^{2+} ions in actual water samples was demonstrated.

Conflicts of interest

There are no conflicts to declare.
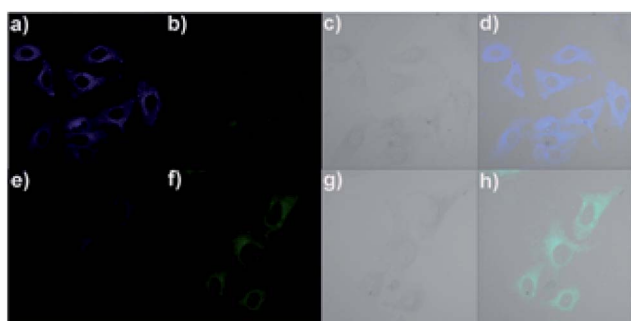
Acknowledgements

Fig. 9 Bright field and fluorescence images of Hela cells stained with the probe RC1. Only the probe RC1: (a) fluorescence image from the blue channel; (b) fluorescence image from the green channel; (c) bright field image; (d) an overlay of the fluorescent blue and green channels and bright-field images. In the presence of Cu^{2+}: (e) fluorescence image from the blue channel; (f) fluorescence image from the green channel; (g) bright field image; (h) an overlay of the fluorescent blue and green channels and bright-field images.

Notes and references

1 S. Angupillai, J.-Y. Hwang, J.-Y. Lee, B. A. Rao and Y.-A. Son, *Sens. Actuators, B*, 2015, **214**, 101.

2 V. Dujols, F. Ford and A. W. Czarnik, *J. Am. Chem. Soc.*, 1997, **119**, 7386.

3 O. García-Beltrán, N. Mena, L. C. Friedrich, J. C. Netto-Ferreira, V. Vargas, F. H. Quina, M. T. Núñez and B. K. Cassels, *Tetrahedron Lett.*, 2012, **53**, 5280.

4 C. Liu, X. Jiao, S. He, L. Zhao and X. Zeng, *Org. Biomol. Chem.*, 2017, **15**, 3947.

5 D. Maity and T. Govindaraju, *Chem.–Eur. J.*, 2011, **17**, 1410.

6 K. Huang, Y. Yue, X. Jiao, C. Liu, Q. Wang, S. He, L. Zhao and X. Zeng, *Dyes Pigm.*, 2017, **143**, 379.

7 T. S. Seeger, F. C. Rosa, C. A. Bizzi, V. L. Dressler, E. M. M. Flores and F. A. Duarte, *Spectrochim. Acta, Part B*, 2015, **105**, 136.

8 Y. Liu, P. Liang and L. Guo, *Talanta*, 2005, **68**, 25.

9 A. A. Ensafi, T. Khayamian, A. Benvidi and E. Mirmomtaz, *Anal. Chim. Acta*, 2006, **561**, 225.

10 J. Wang, D. Larson, N. Foster, S. Armalis, J. Lu, R. Xu, K. Olsen and A. Zirino, *Anal. Chem.*, 1995, **37**, 1481.

11 X. Chen, T. Pradhan, F. Wang, J. S. Kim and J. Yoon, *Chem. Rev.*, 2012, **112**, 1910.

12 Y. Yang, Q. Zhao, W. Feng and F. Li, *Chem. Rev.*, 2013, **113**, 192.

13 M. H. Lee, J. S. Kim and J. L. Sessler, *Chem. Soc. Rev.*, 2015, **44**, 4185.

14 H. Zhu, J. Fan, B. Wang and X. Peng, *Chem. Soc. Rev.*, 2015, **44**, 4337.

15 X. Zhang, Y. Shiraishi and T. Hirai, *Org. Lett.*, 2007, **9**, 5039.

16 M. Yu, M. Shi, Z. Chen, F. Li, X. Li, Y. Gao, J. Xu, H. Yang, Z. Zhou, T. Yi and C. Huang, *Chem.–Eur. J.*, 2008, **14**, 6892.

17 L. Huang, F.-P. Hou, P. Xi, D. Bai, M. Xu, Z. Li, G. Xie, Y. Shi, H. Liu and Z. Zeng, *J. Inorg. Biochem.*, 2011, **105**, 800.

18 L. Tang, F. Li, M. Liu and R. Nandhakumar, *Spectrochim. Acta, Part A*, 2011, **78**, 1168.

19 L. Huang, F. Chen, P. Xi, G. Xie, Z. Li, Y. Shi, M. Xu, H. Liu, Z. Ma, D. Bai and Z. Zeng, *Dyes Pigm.*, 2011, **90**, 265.

20 M.-Z. Tian, M.-M. Hu, J.-L. Fan, X.-J. Peng, J.-Y. Wang, S.-G. Sun and R. Zhang, *Bioorg. Med. Chem. Lett.*, 2013, **23**, 2916.

21 F. Ge, H. Ye, J.-Z. Luo, S. Wang, Y.-J. Sun, B.-X. Zhao and J.-Y. Miao, *Sens. Actuators, B*, 2013, **181**, 215.

22 M. Li, H.-S. Lv, J.-Z. Luo, J.-Y. Miao and B.-X. Zhao, *Sens. Actuators, B*, 2013, **188**, 1235.

23 M. Yu, R. Yuan, C. Shi, W. Zhou, L. Wei and Z. Li, *Dyes Pigm.*, 2013, **99**, 887.

24 S. Goswami, D. Sen, A. K. Das, N. K. Das, K. Aich, H.-K. Fun, C. K. Quah, A. K. Maity and P. Saha, *Sens. Actuators, B*, 2013, **183**, 518.

25 H. Kim, B. A. Rao, J. W. Jeong, S. Mallick, S.-M. Kang, J. S. Choi, C.-S. Lee and Y.-A. Son, *Sens. Actuators, B*, 2015, **210**, 173.

26 E. Wang, Y. Zhou, Q. Huang, L. Pang, H. Qiao, F. Yu, B. Gao, J. Zhang, Y. Min and T. Ma, *Spectrochim. Acta, Part A*, 2016, **152**, 327.

27 Y. Wang, H.-Q. Chang, W.-N. Wu, W.-B. Peng, Y.-F. Yan, C.-M. He, T.-T. Chen, X.-L. Zhao and Z.-Q. Xu, *Sens. Actuators, B*, 2016, **228**, 395.

28 P. Xi, J. Dou, L. Huang, M. Xu, F. Chen, Y. Wu, D. Bai, W. Li and Z. Zeng, *Sens. Actuators, B*, 2010, **148**, 337.

29 X. Chen, J. Jia, H. Ma, S. Wang and X. Wang, *Anal. Chim. Acta*, 2009, **632**, 9.

30 M. Kumar, N. Kumar, V. Bhalla, P. R. Sharma and T. Kaur, *Org. Lett.*, 2012, **14**, 406.

31 L. Yuan, W. Lin, B. Chen and Y. Xie, *Org. Lett.*, 2012, **14**, 432.

32 J. Tang, S. Ma, D. Zhang, Y. Liu, Y. Zhao and Y. Ye, *Sens. Actuators, B*, 2016, **236**, 109.

33 L. Yuan, W. Lin, K. Zheng and S. Zhu, *Acc. Chem. Res.*, 2013, **46**, 1462.

34 G. He, X. Zhang, C. He, X. Zhao and C. Duan, *Tetrahedron*, 2010, **66**, 9762.

35 B. Muthuraj, R. Deshmukh, V. Trivedi and P. K. Iyer, *ACS Appl. Mater. Interfaces*, 2014, **6**, 6562.

36 C. Kar, M. D. Adhikari, A. Ramesh and G. Das, *Inorg. Chem.*, 2013, **52**, 743.

37 Z.-H. Xu, H.-W. Wang, X.-F. Hou, W.-L. Xu, T.-C. Xiang and C.-Z. Wu, *Sens. Actuators, B*, 2014, **201**, 469.

38 Y. Zhou, F. Wang, Y. Kim, S.-J. Kim and J. Yoon, *Org. Lett.*, 2009, **11**, 4442.

39 L. Wang, J. Yan, W. Qin, W. Liu and R. Wang, *Dyes Pigm.*, 2012, **92**, 1083.

40 L. Liu, A. Wang, G. Wang, J. Li and Y. Zhou, *Sens. Actuators, B*, 2015, **215**, 388.

41 V. K. Gupta, N. Mergu and L. K. Kumawat, *Sens. Actuators, B*, 2016, **223**, 101.

42 Y.-K. Yang, K.-J. Yook and J. Tae, *J. Am. Chem. Soc.*, 2005, **127**, 16760.

43 M. Wang, J. Wen, Z. Qin and H. Wang, *Dyes Pigm.*, 2015, **120**, 208.

44 J. Ni, B. Li, L. Zhang, H. Zhao and H. Jiang, *Sens. Actuators, B*, 2015, **215**, 174.

45 Q. Zhou, Z. Wu, X. Huang, F. Zhong and Q. Cai, *Analyst*, 2015, **140**, 6720.

46 G. Li, G. Gao, J. Cheng, X. Chen, Y. Zhao and Y. Ye, *Luminescence*, 2016, **31**, 992.

47 X. Zeng, L. Dong, C. Wu, L. Mu, S.-F. Xue and Z. Tao, *Sens. Actuators, B*, 2009, **141**, 506.

48 N. I. Georgiev, M. D. Dimitrova, A. M. Asiri, K. A. Alamry and V. B. Bojinov, *Dyes Pigm.*, 2015, **115**, 172.

49 S. Guha, S. Lohar, I. Hauli, S. K. Mukhopadhyay and D. Das, *Talanta*, 2011, **85**, 1658.

50 Y. Jiao, L. Zhou, H. He, J. Yin and C. Duan, *Talanta*, 2017, **162**, 403.

51 W.-J. Xu, D.-Q. Qi, J.-Z. You, F.-F. Hu, J.-Y. Bian, C.-X. Yang and J. Huang, *J. Mol. Struct.*, 2015, **1091**, 133.

52 H.-Q. Chang, X.-L. Zhao, W.-N. Wu, L. Jia and Y. Wang, *J. Lumin.*, 2017, **182**, 268.

53 G. M. Sheldrick, *SADABS*, University of Göttingen, Germany, 1996.

54 G. M. Sheldrick, *SHELX-97, Program for the Solution and the Refinement of Crystal Structures*, University of Göttingen, Germany, 1997.

55 W. N. Wu, P. D. Mao, L. Jia, Y. Wang and Z. Q. Xu, *Spectrochim. Acta, Part A*, 2016, **166**, 44.

56 M. J. Frisch, G. W. Trucks, H. B. Schlegel, G. E. Scuseria, M. A. Robb and J. R. Cheeseman, *Gaussian 09, Revision D.01*, Gaussian, Inc., Wallingford CT, 2013.

57 X. Zhang and Y.-Y. Zhu, *Sens. Actuators, B*, 2014, **202**, 609.

58 L.-F. Zhang, J.-L. Zhao, X. Zeng, L. Mu, X.-K. Jiang, M. Deng, J.-X. Zhang and G. Wei, *Sens. Actuators, B*, 2011, **160**, 662.